Journal of African Earth Sciences 206 (2023) 105024

Contents lists available at ScienceDirect

Journal of African Earth Sciences

journal homepage: www.elsevier.com/locate/jafrearsci

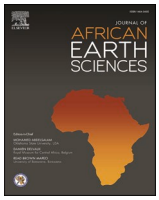

Mineral prospectivity mapping over the Gomoa Area of Ghana's southern Kibi-Winneba belt using support vector machine and naive bayes

Eric Dominic Forson [a,c], Prince Ofori Amponsah [b,*]

[a] Department of Physics, School of Physical and Mathematical Sciences, University of Ghana, Ghana
[b] Department of Earth Science, School of Physical and Mathematical Sciences, University of Ghana, Ghana
[c] University of Tasmania, CODES - ARC Centre of Excellence in Ore Deposits and School of Earth Science, Hobart, Tasmania, 7001, Australia

ARTICLE INFO

Handling Editor: DR Damien Delvaux

Keywords:
Machine learning
Support vector machine
Naive bayes
Geophysics
Remote sensing
Mineral potential mapping

ABSTRACT

Geospatial modeling of mineral prospective regions is essential, owing to its significant contribution towards the development and economic gains of many mineral-endowed countries including, Ghana. Thus, the primary objective of this study is to delineate mineral potential zones in the Gomoa Area of Ghana's southern Kibi-Winneba belt in order to supplement mineral resources in Ghana's existing mineral prospective zones. To achieve the aforementioned objective, researchers generated predictive models characterising gold mineralisation prospects within the study area by employing machine learning techniques comprising support vector machines (SVM) and naive bayes (NB) classifiers on mineral-related conditioning factors. These mineral-related factors (geoscientific thematic layers) were sourced from geophysical, remote sensing, and geological datasets. The resulting mineral prospective models (MPM) produced based on SVM and NB classifiers were exhibited in binary classes (prospective and non-prospective zones). Regions delineated as prospective zones within the study area were, respectively estimated to cover an area extent of 181.62 km^2 and 296.02 km^2 for the SVM-derived MPM and NB-derived MPM and analogously characterise 22.07% and 35.97% of the study area. The ability of these two models to predict was determined using the area under the receiver operating characteristic curve (AUC). The AUC scores obtained for the SVM-derived MPM and the NB-derived MPM were, respectively, 0.90 and 0.83. Outputs of the AUC scores generally indicate that the two models produced have good accuracy, although the SVM-derived MPM performed better than that of the NB-derived MPM. Thus, the machine learning-based mineral prospectivity models produced in this study are worthy outputs to guide the planning of detailed mineral exploration surveys within the study area.

1. Introduction

One of the initial stages of significant relevance in mineral prospecting is to localise various geologically important features associated with the target mineral. Localising these important features is based on the availability and analysis of geological maps made up of lithological units, structures, alteration types, and locations, as well as indicator minerals. In recent years, the evolution of geological mapping methods, including geochemical analysis, coupled with the emergence of remotely sensed geoscientific datasets and advancements in data analytic techniques have gained prominence, particularly in mineral exploration programmes (McKay and Harris, 2016; Bachri et al., 2019; Shirmard et al., 2022). Visualisation, processing, and analysis of these datasets can be carried out with the support of computer and geographic information systems (GIS) approaches (Carranza, 2008; Zeghouane et al., 2016; Zuo et al., 2016; Shabankareh and Hezarkhani, 2017; Amponsah and Forson, 2023). As a consequence, the goal of exploring for minerals by incorporating a variety of geoscientific and geospatial datasets is a multi-criteria decision-making (MCDM) task with the sole purpose of generating a predictive map comprising prospectively delineated zones of the said mineral (known as mineral prospectivity mapping (MPM)) (Forson et al., 2020). Additionally, the use of geoscientific information in MPM based on machine learning (ML) algorithms helps mineral exploration geoscientists overcome common challenges associated with traditional methods (where the influence or weight of various thematic layers used is determined in a subjective manner) due to over-reliance on expert opinions (examples include PROMETHEE (Abedi et al., 2012b), the Analytical Hierarchy Process

* Corresponding author.
E-mail address: pamponsah@ug.edu.gh (P.O. Amponsah).

https://doi.org/10.1016/j.jafrearsci.2023.105024
Received 25 January 2023; Received in revised form 1 August 2023; Accepted 1 August 2023
Available online 5 August 2023

(AHP; Du et al., 2016), Fuzzy AHP (Forson et al., 2020; Amponsah et al., 2022b), and the best-worst method (Forson and Menyeh, 2023)). The use of machine learning methods are devoid of this aforesaid subjectivity, and thus, the influence of the various thematic layers used are determined by assessing the spatial correlation of the thematic layers used with respect to the target labels (occurrences). Notwithstanding the difficulty associated with generating reliable models in geoscience owing to the inhomogeneity of the Earth (Zhan et al., 2023), these ML algorithms also help reduce exploration costs, particularly over barren or under-explored terrains, because of their capacity to classify the mineral prospects over an area into favourable and non-favourable zones (Shirmard et al., 2022). Thus, machine learning techniques have also been found applicable by geoscientists in hydrocarbon exploration (Zhang et al., 2021; Cheng and Fu, 2022), groundwater exploration (Liu et al., 2023; Al-Kindi and Janizadeh, 2022), and geohazard monitoring (Cao et al., 2020; Ma et al., 2022). Classification based on machine learning algorithms generally come in two forms: supervised and unsupervised classifications. ML-based supervised classification uses training data containing locations of known mineral deposits and non-mineral deposits and a set of thematic layers extracted from geoscientific datasets (also referred to as predictors) to classify potential zones of mineral occurrences over an area of interest (Sun et al., 2019, 2020). However, with unsupervised classification, the mineral potential orientation over an area is classified based on the feature statistics of each of the geoscientific thematic layers used (Zuo and Carranza, 2011). In the supervised classification of prospectively viable zones of mineral occurrences over an area, machine learning offers several classifiers that can be employed. Application of supervised ML classifiers in carrying out mineral prospectivity mapping over various geologic environments continues to rise in recent years owing to their ability to produce efficient mineral prospectivity models that can be essential to guide future mineral exploration activities (Abedi et al., 2012a; Zeghouane et al., 2016; Shabankareh and Hezarkhani, 2017; Sun et al., 2019, 2020; Parsa and Maghsoudi, 2021). It is worth acknowledging that each of these ML classifiers have their respective strengths and weaknesses and may be more or less suitable than the other in classifying the presence or absence of a particular mineral based on the geological terrane as well as the context of the exploration (Zuo and Carranza, 2011). The inference from this assertion by Zuo and Carranza (2011) suggests that for best practices in MPM over a particular region of interest, the use of two or more ML classifiers is commendable. Thus, model comparison for mineral prospectivity mapping has been found applicable in other geological terranes (Rodriguez-Galiano et al., 2015; Saberioon et al., 2018; Cardoso-Fernandes et al., 2019).

Of all the gold belts in Ghana, it is the southern Kibi-Winneba belt (SKWB) where the study area falls, that is less explored in terms of its prospectivity in spite of its geological resemblance with the Ashanti belt. In an attempt to unravel the mineral prospects over the belt, knowledge-driven (Fuzzy analytical hierarchy process (Forson et al., 2020) and Best-worst method (Forson and Menyeh, 2023)) methods have been used to delineate the mineral prospects of the area. Taking into cognisance the superiority of machine learning models over these aforementioned techniques employed over the area (Shirmard et al., 2022), the objective of this present study is to delineate the mineral prospects over the Gomoa Area of the SKWB using thirteen (13) thematic layers extracted from geophysical, geological, and remotely sensed datasets based on two machine-learning models comprising support vector machine (SVM) and naive bayes (NB) classifiers. The choice of the NB classifier as a suitable ML algorithm for generating the MPM model in this study is guided by its ability to perform well with multi-source thematic layers as well as fewer training datasets (which is the case in this study) and has been employed in the western part of India (Porwal et al., 2006) and other geological terranes (Bérubé et al., 2018; Bédard et al., 2022). SVM is fundamentally a two-class classifier, coupled with its application in several geological terranes (Zuo and Carranza, 2011; Abedi et al., 2012a; Rodriguez-Galiano et al., 2015; Shabankareh and Hezarkhani, 2017), it was also selected as to produce a MPM in this study. Also, thematic layers sourced from geophysical, geological, and remote sensing datasets were chosen for this study owing to their capability in delineating alteration zones, indicator minerals (such as pyrite, arsenopyrite, magnetite, and chalcopyrite), as well as lineaments associated with gold mineralisation within the study area (Klemd et al., 2002; Forson et al., 2021). It is expected that the outcome of this study will contribute to efforts geared towards unravelling the mineral potential of the SKWB.

2. Study area and geological setting

2.1. Study area description

The 823 km^2 study area (Fig. 1) is located in the Central Region of Ghana, 122 km southwest of Accra, the country's capital, and spans between the Gomoa East, west, and Ekumfi districts along the Atlantic coast of the Gulf of Guinea. The study area is bounded by the coordinates 730,000 mE, 610,000 mN and 754,000 mE, 586,000 mN within the World Geodetic System 1984 (WGS84) datum.

2.2. Geological setting

According to the current 1:1,000,000 geological map published by Agyei Duodu et al. (2009), the area under consideration is mainly underlain by the southern portion of the Kibi-Winneba belt (Fig. 2), with small portions to the east and west underlain by the southern portions of the Suhum and Cape-Coast basins, respectively. The Kibi-Winneba belt, which outcrops in the study area, is part of several linear arcuate greenstone belts which defines the architecture of the Birimian Paleoproterozoic terrane in Ghana (Leube et al., 1990; Jessell et al., 2012; Amponsah et al., 2015, 2016; Salvi et al., 2016; Feng et al., 2018, 2019; Asiedu et al., 2019; Sapah et al., 2021; Nunoo et al., 2022; Amponsah et al., 2023) formed during the Eburnean orogeny (Bonhomme, 1962; Baratoux et al., 2011). Rocks that crop out within the belt include amphibolites, volcaniclastics, and volcanic flows with bimodal tholeiitic and calc-alkaline affinities (Anum et al., 2015; Forson et al., 2020). The tholeiitic basalts predate the calc-alkaline series and represent an immature volcanic arc setting (Ama Salah et al., 1996; Béziat et al., 2000; Lüdtke et al., 2000; Diatta et al., 2017). Volcanism from radiometric dating in the Birimian terrane shows that volcanism peaked around 2190 - 2160 Ma (Davis et al., 1994). Syn-tectonically intruding the mafic volcanites above are the 2113 ± 1 Ma biotite granites with Archean signatures (Davis et al., 1994; Agyei Duodu et al., 2009) and the 2116 ± 2 Ma biotite (hornblende muscovite) granitoid. Unconformably overlying the volcanites is the molassic deposit Tarkwaian sediments,

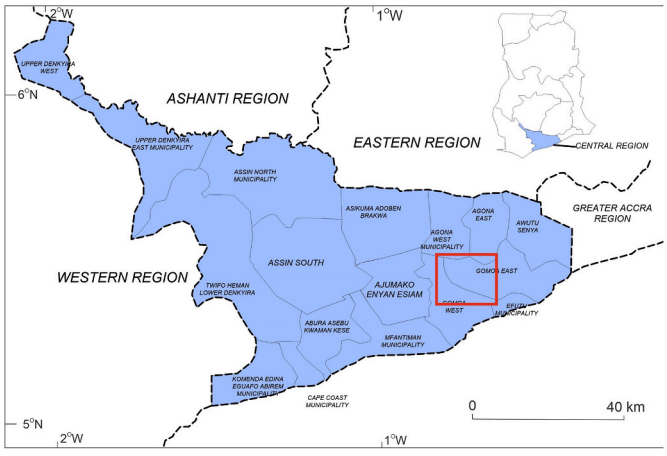

Fig. 1. Map of the Central Region of Ghana showing various administrative districts (Study area is marked in red).

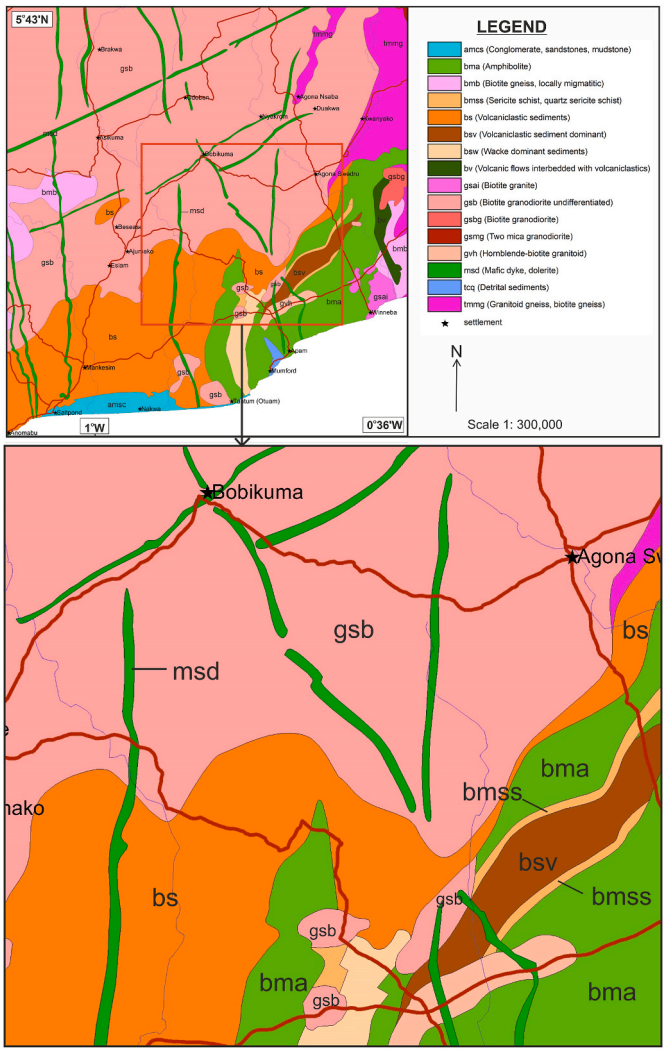

Fig. 2. Modified geological map of the study area (Agyei Duodu et al., 2009).

composed of detrital sediments dominated by sandstones and conglomerates. The granitoid complex Suhum Basin (Agyei Duodu et al., 2009) occurs to the east of the Kibi-Winneba belt as well as in the study area and is composed of four types of granitoids. Type 1 is composed of biotite gneisses with subordinate biotite schist dated around 2165 ± 9 Ma (Opare-Addo et al., 1993), while the Type 2 granitoid in the basin was emplaced around 2134 ± 4 Ma (Agyei Duodu et al., 2009). Types 1 and 2 granitoids have been intruded by both the 2106 ± 1 Ma K-feldspar rich Type 3 granitoid and the 2088 ± 1 Ma Type 4 two mica granites (Hirdes et al., 1992). Juxtaposing the southern Kibi-Winneba belt to the west is the southern Cape Coast basin. The southern Cape Coast basin is underlain by 2187 ± 1 Ma biotite gneisses, biotite schist and the 2116 ± 1 Ma to 2102 ± 1 Ma two mica (hornblende) granitoid intrusives. All the rocks in the study area have been intruded by later Mesozoic mafic dolerite dykes. The tectonic evolution of the Birimian terrane has been described by many workers as polycyclic events (Ledru et al., 1988; Hirdes et al., 1992; Milési et al., 1992; Feybesse et al., 2006). This paper will adopt the structural interpretation of Feybesse et al. (2006). Feybesse et al. (2006) identified three phases of deformation within the Birimian terrane in Ghana. The first deformation event, termed D1 deformation, is defined by S1 foliation, which is parallel to the axial plane of F1 microfolds, and by an L1 stretching lineation. Foliations observed during this stage differ in accordance with the intensity of metamorphism and the coaxial strain associated with the deformation. Where the evidence of simple shear strain was pronounced stretching lineations and symmetrical pressure shadows were produced. The transposition of bedding was not associated with the strain type produced during this deformation. The D2 deformational event is characterized by maximum strain, which is manifested by F2 folds with horizontal or slightly plunging hinges, associated with a general east-northeast to west-southwest striking S2 cleavages and north-east to south-west sinistral ductile faults with reverse components. D3 is defined by folds generally associated with brittle shears, indicating that the crust was already exhumed to higher structural levels (Amponsah et al., 2016).

2.3. Gold mineralisation style

Gold mineralisation in the Kibi-Winneba belt is structurally controlled and occurs mainly in second-order structures, usually 10–15 km of the main crustal-scale transcurrent shear zone. On the deposit scale, gold in the belt is hosted in intensely sheared and tightly folded volcanoclastic rocks (which are lithofacies controlled) or in chemical sediments usually intruded by syn-tectonic and late Eburnean age felsic, mafic, and intermediate dykes or as quartz-albite-carbonate-sulphide lodes or tensional stockworks usually developed at the margins of the dykes (Xtra-Gold Resource Corporation, 2021). Arsenopyrite in the metasediments and metavolcanics, as well as pyrites within the plutonic rocks, are the predominant sulphide minerals that control gold mineralisation in the area. These sulphides are mostly associated with regional greenschist facies metamorphism. The wall-rock alteration associated with the mineralisation zone in the metasediments are carbonitization, sulphidation and graphite formation through the reduction of CO_2, CO and CH_4 (Leube et al., 1990), dolomitization, and sericitization, whilst in the plutonic rock, k-feldspar alteration and mylonitization are key. Other sulphides associated with the gold mineralisation zones are pyrrhotite, chalcopyrite, marcasite, rutile, xenotime, bornite, and galena. Gold does occur as free gold within the vein selveges with the wall rocks or is interlocked as refractory gold within the lattices of the arsenopyrite and pyrites (Leube et al., 1990; Xtra-Gold Resource Corporation, 2021). Furthermore, hydrothermal gold mineralisation in the study area is mostly quartz-veins hosted in close association with disseminated auriferous sulphide and is therefore mostly structurally controlled. These quartz veins occur in steeply dipping shear zone contacts or boundaries between the meta-sediments and metavolcanics, or mostly as stockwork fracture-controlled quartz veins within the late plutons, which intruded the metasediments (bsv and bmss) and metavolcanics (bv and bma). These shear zones act as fluid plumbing systems and therefore control the path of gold mineralisation (Leube et al., 1990).

3. Materials and methods

3.1. Geoscientific thematic layers

In carrying out predictive modeling for gold prospects over a designated area, the use of geoscientific-based thematic layers are essential because they are decisive conditional factors. In choosing various geoscientific thematic layers that are to be included in a mineral predictive modeling exercise over an area of interest, an understanding of the mineralisation style of the said area is required. Thus, thirteen geoscientific-based thematic layers were derived from geophysical, geological, and remote sensing datasets that had been obtained from reputable and publicly accessible institutions. The geophysical dataset, which comprises airborne magnetics and airborne radiometrics together with the geological data, was obtained from the Ghana Geological Survey Authority. The gravity dataset used was obtained from the GFZ German Research Centre for Geoscience (www.gfz-potsdam.de). The main remote sensing data used (obtained from the United States Geological Survey Earth Resources Observation and Science Centre) in this study was based on data acquired by the Landsat 8 Operational Land Imager (OLI). From the geological data, the various lithologies within

the study area were derived in ArcGIS 10.4 environment. By using the Geosoft Oasis Montaj software, each of the three radiometric elements (potassium (K), thorium (eTh) and uranium (eU)) were gridded. Afterwards, two radiometric channel ratios (K-eTh and eU-eTh ratios) were further generated by using the individual radioelements as inputs. In all, five layers were derived from the radiometric data. For the airborne magnetic data, various preprocessing and processing procedures were carried out in the Geosoft Oasis Montaj, including regional-residual separation to generate the residual magnetic intensity (RMI) grid. The study area lies in a low magnetic latitude region and thus the RMI was reduced to the magnetic pole to generate the reduction-to-pole (RTP) magnetic intensity layer. By applying the analytic signal (AS) on the RMI and the first vertical derivative (FVD) filters on the RTP grid, the AS (which determines the distribution of the magnetic intensity gradient) and FVD (determines the rate at which the magnetic field changes in the vertical direction and subsequently enhances the resolution of closely spaced magnetic anomalies) layers were respectively generated. The lineament density (LD) layer (which comprises the occurrence of lineaments such as faults, fractures, foliations, dykes, etc. with respect to a given area) was also derived by applying the Centre for Exploration Targeting (CET) grid analysis technique on the RMI grid. In the case of the Bouguer anomaly data, regional-residual separation was carried out to obtain the residual gravity layer. In the case of the Landsat 8 OLI imagery data, an atmospheric correction was first carried out on the remote sensing data to remove various effects that may have been induced by the atmosphere on the reflectance values of the remote sensing images (Forson et al., 2021). Radiometric correction was, however, not applied since the acquisition of the data was at L1C (radiance to the sensor) without cloud cover. Afterwards, two layers of band ratios B4/B2 and B6/B7 which respectively elucidate iron and hydroxyl alteration zones within the study area, were generated in QGIS software. After carrying out the various processing procedures that are vital towards the generation of the thematic layers, the geological layer which was originally in a vector format was also transformed into a raster. Afterwards, each of these thirteen thematic layers were imported into a GIS environment and were subsequently resampled to a cell resolution of 75 m, resulting in a grid of 146,316 pixels in an R programming environment. To efficiently integrate these thematic layers (shown in Figs. 3(a-f), 4(a-f), and 5) towards the production of a mineral prospectivity model based on the machine learning classifiers to be used, the original values of each of these thematic layers were normalised to confine them within a range of 0–1 as shown in equation (1).

$$TM_{norm} = \frac{TM - TM_{\min}}{TM_{\max} - TM_{\min}} \quad (1)$$

TM is the geoscientific thematic layer that is to be normalised; TM_{min} and TM_{max} depict, respectively, the minimum and maximum values of the chosen geoscientific thematic layer (TM). TM_{norm} is the normalised layer, with values ranging from 0 to 1.

It is noteworthy that the layers derived from the magnetic data are useful in mapping anomalously high magnetic regions (which could be due to indicator minerals such as arsenopyrite, pyrite, and magnetite) (Forson et al., 2020). The gravity layer has the capacity to delineate bulk mineral deposits associated with sulphide minerals such as arsenopyrite, chalcopyrite, and pyrite (Forson et al., 2021). Radiometrically derived layers used in this study are essential in mapping out hydrothermal alteration zones with significant relevance towards mineralisation occurrences within the study area. The remote sensing-derived layers (OH and Fe concentration) also characterise sericite, chalcopyrite, and argillite associated minerals with association to gold mineralisation within the study area (Klemd et al., 2002; Forson et al., 2021).

3.2. Training and testing data

Mineral deposit occurrence is a dichotomous variable that is expressed in terms of target labels with a value of 0 for non-deposit occurrence and 1 for deposit occurrence when carrying out the training and testing procedures (Carranza and Laborte, 2016). In this

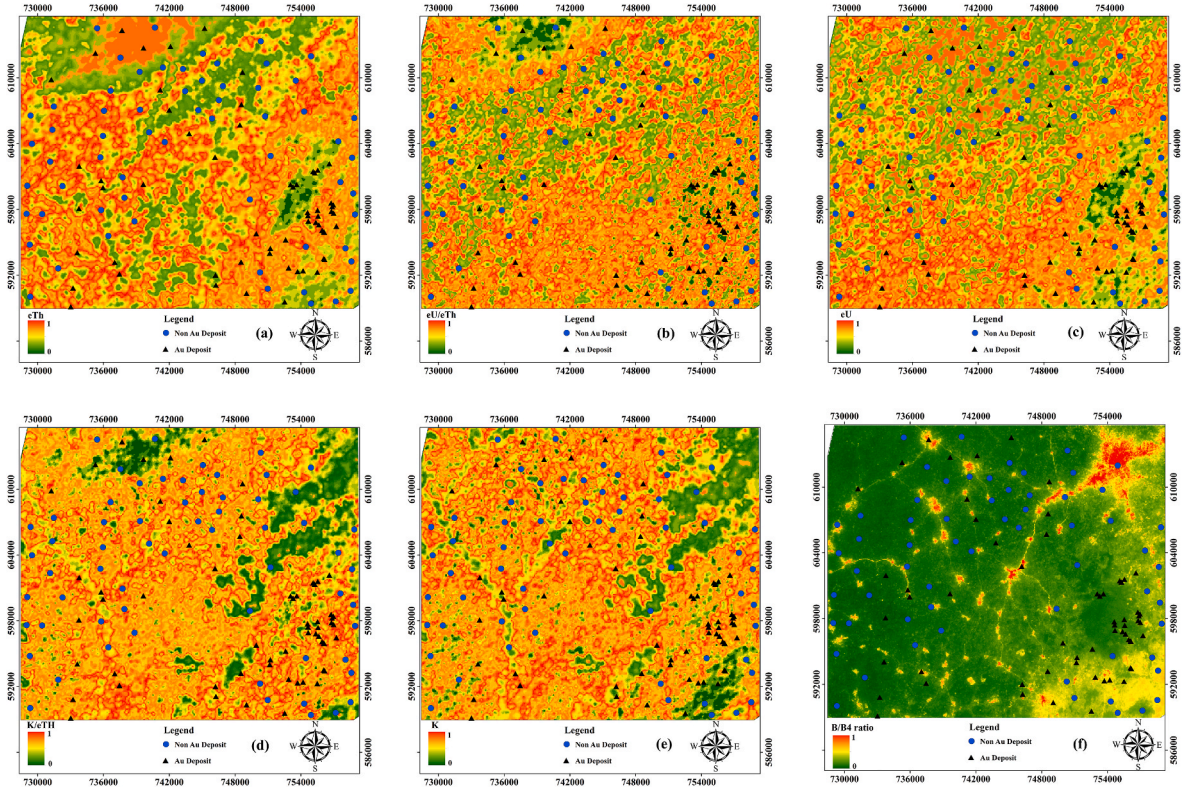

Fig. 3. Normalised image of (a) eTh concentration layer (b) eU/eTh ratio layer (c) eU concentration layer (d) K/eTh ratio layer (e) K concentration layer (f) Fe concentration layer.

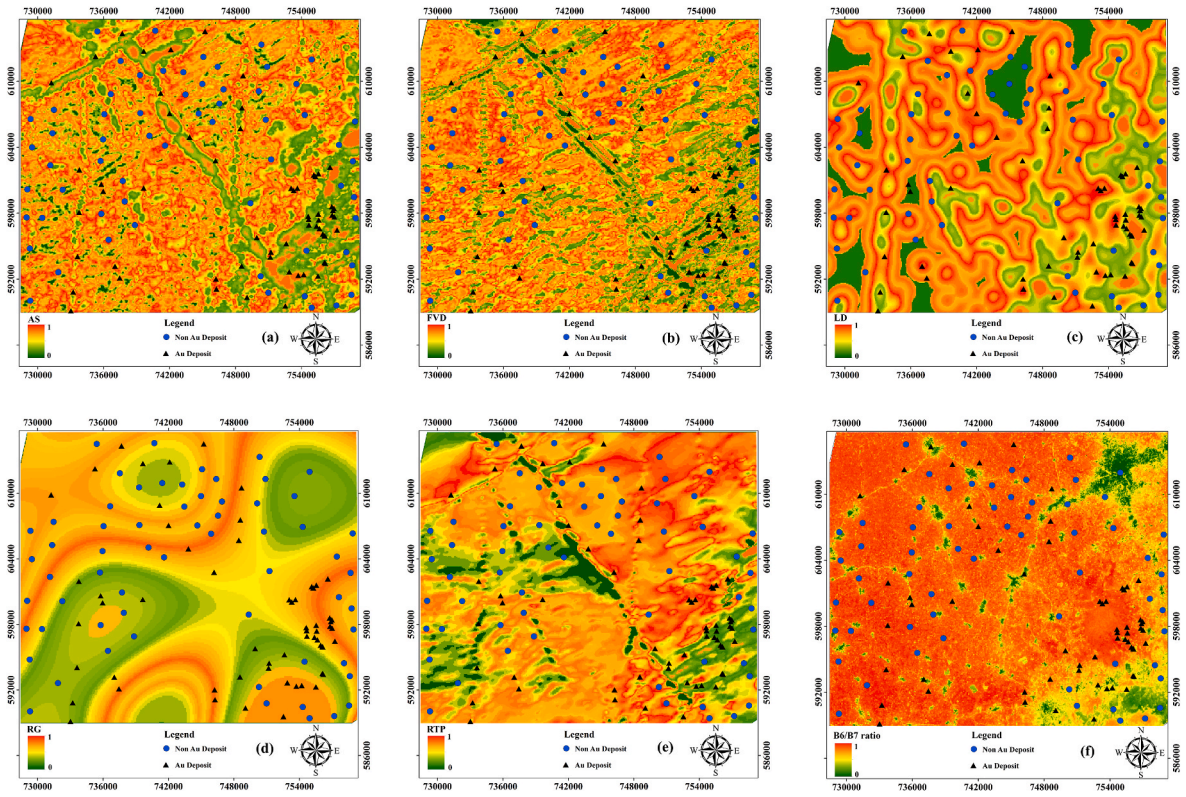

Fig. 4. Normalised image of (a) Analytic signal layer (b) First vertical derivative layer (c) Lineament density layer (d) Residual gravity layer (e) RTP magnetic intensity layer (f) Hydroxyl (OH) concentration layer.

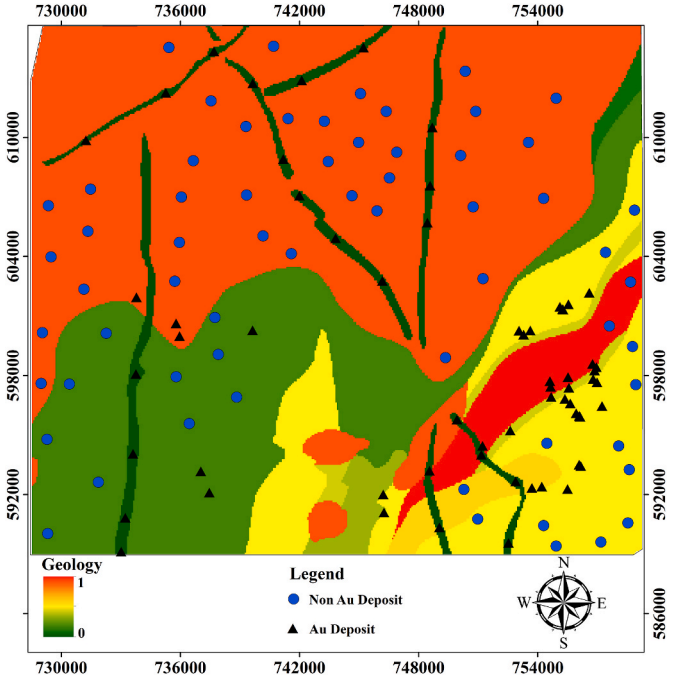

Fig. 5. Normalised geological layer.

study, 60 known locations of Au occurrence (Dove, 1991; Newmont Ghana Limited, 2006; Geodita Resources Ltd, 2007; 2012, 2013) within the Gomoa Area of the Southern Kibi-Winneba Belt were employed to represent the Au deposit occurrence. For the non-Au deposit occurrences, the location of the samples was chosen per the procedure outlined by Carranza et al. (2008) and Zuo and Carranza (2011). The first step in the aforementioned procedure that governs the selection of non-Au deposit sample locations dwells on the premise that the number of non-Au deposit locations should be the same as the number of Au deposit locations. This first procedure balances the negative and positive samples within the training and testing datasets to be employed in the generation of the mineral predictive model. In the second procedure, the locations of the non-Au deposits that would be selected should be situated such that they are distal from any known Au deposit location; this is because locations that are nearer to the Au deposit locations are more likely to possess synonymous mineralisation conditions. In this study, point pattern analysis was carried out to ascertain the sufficient distance beyond which the locations of non-Au deposit occurrence should be chosen owing to its usefulness in visualising and interpreting the spatial distribution patterns within point data (Zhang and Liu, 2019). Thus, for any two Au deposit occurrences, the maximum distance between them was statistically computed to be 1609 m using the average nearest neighbour analysis technique. This indicates that, for each location of the Au deposit, there is a 100% possibility of finding another Au occurrence within a 1609 m circumference around it. Non-Au deposit occurrences should be located beyond the 1609 m distance. It is noteworthy that only a few locations can be chosen within the aforementioned range, and thus, a buffer distance of 1312 m, within which there is an 82% possibility of finding a neighbouring gold deposit close to any given Au deposit was selected. The third step of the aforementioned procedure concerns the fact that mineral occurrences within an area of interest are distributed in a spatially clustered manner, because they are products whose occurrence is scarce and within non-random ore-forming processes. Contrary to this, the locations of non-Au deposits selected should be spatially distributed in a random fashion as they result from common geological processes. From the three steps outlined, 60 non-Au deposit locations were selected randomly to attain a dichotomously balanced target labels. The target labels were then split into two, representing respectively the training data (70% of the target labels) and

testing data (30% of the target labels). The training data was employed in generating the predictive models whereas the testing data was used to assess the performance of the predictive models generated.

3.3. Classifiers

In this study, two machine learning-based supervised classification algorithmss have been employed, and they encompass the naive bayes and support vector machine.

3.3.1. Naive bayes classifier

The naive bayes classifier fundamentally dwells on the likelihood of occurrence of a particular event; in this present study, it can analogously be associated with the probability of occurrence of a mineral deposit over the study area, with prior knowledge learned from the training data (Bédard et al., 2022). In delineating mineral prospective zones based on the naive bayes classifier, class probabilities for each target (occurrence or non-occurrence) are calculated, and the observation is classified based on the class with the highest probability. Although this classifier primarily functions based on the assumption of independence among the geospatial layers (predictors), it still exhibits good predictive ability even in instances where the predictors violate the independence rule (Bédard et al., 2022). Implementation of the naive nayes classifier for mineral prospectivity mapping in our present study was carried out in the Python programming language.

3.3.2. Support vector machine classifier

The support vector machine (SVM) is a supervised machine learning-based classifier essential for maximising the capacity of various mathematical functions with a particular set of datasets (Noble, 2006; Li and Sun, 2020). This classifier, which was originally proposed by Vapnik (1999), has in recent years been employed successfully in mineral prospecting in many areas based on remote sensing, geophysical, and other mineral-related geoscientific datasets (Abedi et al., 2012a; Rodriguez-Galiano et al., 2015; Chen and Wu, 2017; Shabankareh and Hezarkhani, 2017). Supervised classification based on the SVM classifier was carried out in Python based on kernel functions comprising linear, polynomial, radial basis function (rbf) and sigmoid. The fundamental principle which underlies the SVM classifier can be found in many recent works of literature (Rodriguez-Galiano et al., 2015; De Boissieu et al., 2018; Cardoso-Fernandes et al., 2020). In this study, the rbf kernel function with a penalty parameter and gamma values of 10 and 0.1, respectively, were identified as the most efficient parameters for the classification. This penalty parameter was essential, particularly in dealing with non-separable classes during the classification.

3.4. Training and evaluation of the models

In this study, the generation of input data, which comprises the thematic layers and the Au target labels were succeeded by the production of SVM and NB-based machine learning models through a training process. The training process primarily deals with determining the essential parameters for the machine learning models to be generated. During data-driven modeling, specifying parameters for a priori fitting configuration is very strenuous because the attainment of optimal parameters for various machine learning models differ with respect to the input dataset used. This presupposes that the determination of these aforementioned parameters does not rely on any empirical rule that is universal in nature, and thus, a less subjective trial-and-error procedure is required to invariably attain optimal parameters. In this study, the trial-and-error procedure was carried out by applying the grid search cross-validation (cv) technique with reference to previous studies (Rodriguez-Galiano et al., 2015; Bérubé et al., 2018; Cardoso-Fernandes et al., 2020; Pham et al., 2021; Bédard et al., 2022), as summarized in Table 1. By carrying out this technique, the optimal parameters that were attained (which have been summarized in Table 2) were used in training each of the two machine learning models incorporated in this study. The classification performance of each of the machine learning models was assessed by implementing a 10-fold cross-validation procedure which employs their respective optimal parameters attained based on the grid search cv approach.

Table 1
Parameter ranges for training the machine learning models.

Machine learning model	Parameter	Parameter Description	Chosen Range
Support vector machine	Cost (C)	Is the penalty factor due to misclassification error	0.01–100
	Kernel	Transforms dataset that are linearly insparable to linearly separable data	poly, rbf, sigmoid
	Gamma	Outlines the degree of influence associated with each training example	1e-4 - 1.0
Naive bayes	priors	Prior probabilities of the classes	None
	var_smoothing	Portion of the largest variance of all features that is added to variances for calculation stability	1e-09 - 1

Table 2
Optimum parameters for training the machine learning models using the Grid Search CV.

Machine Learning Model	Parameter	Chosen Optimal Parameter Value
Support vector machine	Cost (C)	10
	Kernel	rbf
	Gamma	0.1
Naive bayes	priors	None
	var_smoothing	0.00231012970008316

To assess the importance of each thematic layer towards the MPM models to be generated based on the SVM and NB, the permutation feature importance was carried out using the testing data. For a given number of layers, the permutation importance tool, which is hosted in the scikit-learn library, computes the feature importance of each layer as expressed in equation (2) (Pedregosa et al., 2011).

$$i_j = s - \frac{1}{K}\sum_{k=1}^{K} s_{k,j} \tag{2}$$

Where i_j is the computed permutation importance for each layer, s and $s_{k,j}$ represent the scores of the model, K is a the number of repetitions observed and k is a repetitive value within a number of repetitions.

In predictive modeling, the efficacy of the natural resource (groundwater or mineral) to be predicted ought to be evaluated to build confidence in the outputs generated (Amponsah et al., 2022a). For this reason, the mineral prospectivity models generated based on the support vector machine and naive bayes classifiers were assessed by using the receiver operating characteristics (ROC) curve to determine the spatial correlation between the mineral-based predictive models produced and Au mineralisation occurrence within the study area by using the testing data. On a typical ROC curve, the abscissa characterises the false positive rate (FPR) (analogous to 1 specificity) as expressed in equation (3) (Sun et al., 2020). Along the ordinate is the true positive rate (TPR), which is analogously referred to as sensitivity and is expressed in equation (3). A determination of the spatial relationship between the predictive models generated and the testing datasets was carried out based on the area under the ROC curves (AUC) obtained. Higher values of AUC depict a strong spatial association between the predictive models and the testing target labels within the study area.

$$FPR = \frac{FP}{TN + FP} \tag{3}$$

$$TPR = \frac{TP}{FN + TP} \tag{4}$$

From equations (3) and (4), FP, TN, TP, and FN characterises, respectively, the false positives, true negatives, true positives, and false negatives. Furthermore, model evaluation indices comprising precision (a quality determinant of positive predictions made by a model is expressed in equation (5)), recall (shown in equation (6) represents the fraction of data samples that are correctly identified by a predictive model for a given class), accuracy (expressed in equation (7) depicts the percentage of correct predictions made by a model), and F1 score (which characterises a predictive model's accuracy and it is expressed in equation (8)) were also used to evaluate the performance of the mineral prospectivity models generated.

$$Precision = \frac{TP}{TP + FP} \tag{5}$$

$$Recall = \frac{TP}{TP + FN} \tag{6}$$

$$Accuracy = \frac{TP + TN}{TP + TN + FP + FN} \tag{7}$$

$$F1\ Score = 2\ x\ \left[\frac{Precision\ x\ Recall}{Precision + Recall}\right] \tag{8}$$

4. Results and discussion

4.1. Relevance of the mineral potential factors

The predictive modeling results obtained based on the use of the support vector machine and the naive bayes classifiers were interpreted by carrying out a quantitative computation of the relative importance of each of the mineral potential factors (Fig. 3(a), (b), 3(c), 3(d), 3(e), 3(f), 4(a), 4(b), 4(c), 4(d), 4(e), 4(f) and 5) towards the generation of the mineral prospectivity models. By carrying out permutation feature importance on each of the two predictive models generated, the contribution and influence of each of the thematic features towards the MPMs generated were determined (shown in Fig. 6). In the case of the mineral prospectivity model produced based on the SVM classifier (Fig. 7(a)), the lineament density and K/eTh ratio predictors make the most contribution towards the SVM-based MPM (shown in Fig. 6). This is orderly preceded by residual gravity, analytic signal, geology, RTP, eU/eTh ratio, eU concentration, first vertical derivative (FVD), hydroxyl (OH) concentration, iron (Fe) concentration, and potassium (K) concentration predictors, as shown in Fig. 6(b). In the SVM-based MPM, the eTh concentration predictor is the feature with the least contribution towards the predictive model generated. For the NB-based MPM (Fig. 7 (b)), it is the geology feature that made the optimum contribution towards the predictive model generated, followed by RG, RTP, LD, K/eTh, AS, eU concentration, OH concentration, eU/eTh ratio, Fe concentration, FVD, K concentration, and eTh concentration features, as shown in Fig. 6. For both mineral prospectivity models produced, thematic features comprising AS, K/eTh, geology, OH, lineament density, residual gravity, uranium concentration, and RTP were generally observed to impose enormous influence on the predictive models. This corroborates the literature assertion that the mineralisation within the study area is associated with magnetically high indicator minerals such as magnetite and thus is influenced by the RTP and analytic signal magnetic features (Forson et al., 2021). These magnetite ores often contain sulphide minerals comprising arsenopyrite, pyrite, and chalcopyrite. In the upper greenschist metamorphic zones within the granitoids, pyrite to pyrrhotite as well as amphibole-bearing minerals exhibit high magnetic responses, making the contribution of the RTP and AS very essential to the outputs generated (Perrouty et al., 2012; Forson et al., 2022b). Also, the residual gravity feature's influence could be due to the premise that these sulphide indicator minerals, comprising arsenopyrite, chalcopyrite, pyrite, and pyrrhotite are iron-predominated and are most likely to be associated with high specific gravity (Klemd et al., 2002; Forson et al., 2021). The significant influence observed by the eU concentration affirms the literature findings that anomalously high regions of uranium concentration characterise regions where gold mineralisation is likely to occur (Forson et al., 2021). The potassium-thorium (K/eTh) layer, which was also observed to have a significant influence in the models generated, could be due to potassium-thorium antagonism (due to a rise in potassium and a decline in thorium concentration), resulting in the occurrence of alteration zones that are essential targets for mineralisation occurrence (Wemegah et al., 2015; Forson et al., 2021). The significant contribution by the lineament density feature towards the predictive models is also expected because, in the study area, quartz vein mineralisations have been association with geological structures such as faults, folds and dykes (Klemd et al., 2002; Forson et al., 2021). The relevance of geology in mineralisation occurrences cannot be underestimated, and thus the observation that it is highly significant towards the SVM-based MPM and the NB-based MPM is expected. Within the study area, hydroxyl-bearing minerals such as illite, goethite, limonite, and sericite are observed within adjacently lying country rocks with carbonate-chalcopyrite-arsenopyrite-gold-tourmaline-sericite accumulations (Klemd et al., 2002; Dzigbodi-Adjimah, 2004). Thus, the significant contribution of the hydroxyl (OH) feature towards the predictive models generated is expected. In both predictive models generated, the potassium concentration feature was observed to exhibit low significance. This corroborates with a study by Forson et al. (2022b), which observed the potassium concentration feature as a non-indicator feature to gold mineralisation over the southern Kibi-Winneba belt. The relevance of these thematic features towards gold mineralisation prospects may facilitate future gold prospecting and provide insights into the model that characterises gold mineralisation within the study area.

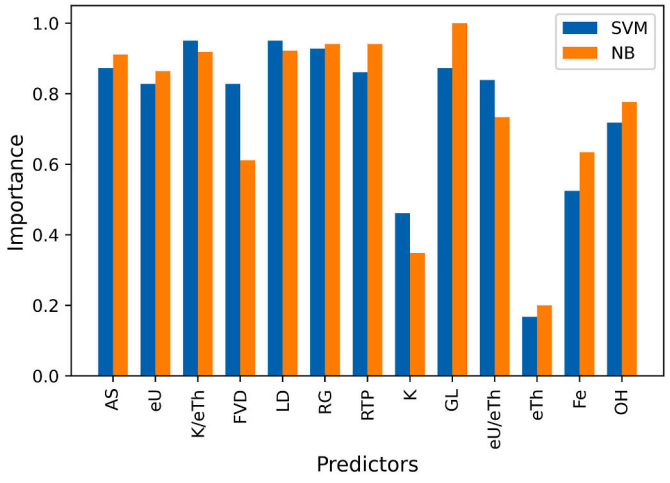

Fig. 6. Feature importance of thematic layers towards SVM-based MPM and NB-based MPM produced.

4.2. Mineral prospectivity models (MPMs)

To assist in the production of a predictive model that delineates various regions within the study area that are prospective and non-prospective to gold mineralisation, the support vector machine and the naive bayes classifiers were employed on the thirteen thematic features derived from geological, remote sensing, and geophysical layers. Output for each of the predictive models was discretised into two classes comprising prospective (regions with mineral potential capacity) and non-prospective (regions deemed to exhibit minimal or no potential of the sought-after mineral deposit) areas. For the mineral prospectivity model produced based on the SVM classifier (shown in Fig. 7(b)),

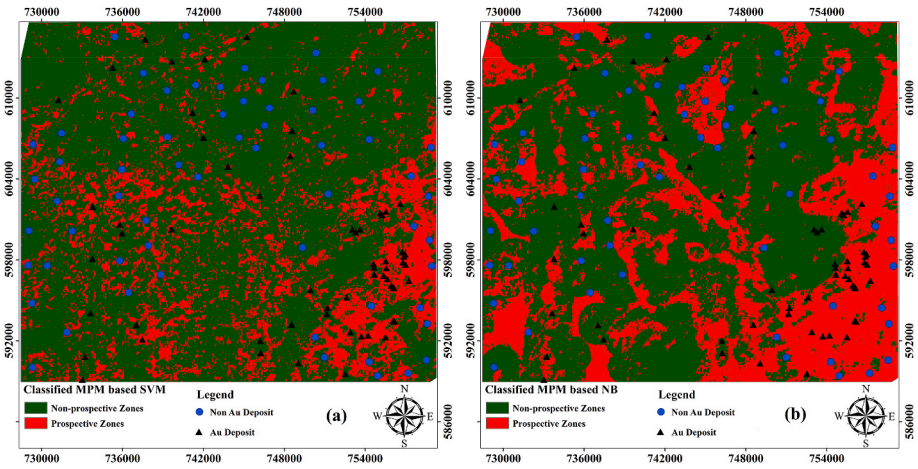

Fig. 7. Mineral prospectivity models based on (a) support vector Machine classifier (b) naive bayes classifier.

regions delineated as prospective cover an areal extent of 181.62 km^2 (analogous to 22.07% of the total size of the study area), whereas the non-prospective class was observed to cover an area of 641.41 km^2, representing 77.93% of the total study area size. The prospective regions within the SVM-based MPM were predominantly observed within the southeastern part of the study area. With respect to the naive bayes-based mineral prospectivity model (Fig. 7(a)), 35.97% (representing 296.02 km^2) of the total study area extent has been delineated to comprise the prospective class, whereas the remaining portion of the study area (made up of 527.01 km^2) characterises regions delineated as non-prospective to gold mineralisation. It can be observed from the NB-based MPM that the prospective class generally characterises the eastern, western, southeastern and the central portions of the study area. In general, the southeastern portion, which was delineated as prospective on both predictive models, falls within the Birimian metavolcanics terrane, known to be associated with high prospects for gold mineralisation occurrence within the study area (Klemd et al., 2002).

4.3. Evaluation of the mineral prospectivity models

To make the predictive models generated essentially reliable for any further deductions, interpretations, and usage by various geoscientists, they ought to be evaluated to determine their efficacy and accuracy. Evaluating predictive models makes them worthy for decision-making and builds confidence in users of those models (Forson et al., 2022a). In this regard, the predictive efficacy of the mineral prospectivity models generated based on the SVM and NB classifiers was evaluated using the receiver operating characteristics (ROC) curve. The scores obtained for the area under the ROC curve (AUC) for the MPM results produced by the SVM classifier and NB classifier are, respectively, 0.90 and 0.83 (as shown in Fig. 8). Results obtained for the AUC scores explicitly indicate that the MPM results produced by the support vector machine classifier perform better than the predictive model generated by the naive bayes classifier. This analogously stipulates that, the mineral prospectivity models created by employing the SVM classifier obtained the highest accuracy while predicting the prospective zones within the study area that possess gold mineralisation occurrences. Results obtained for the performance metrics (precision, recall, accuracy, and the f1 score) indicate a generally enhanced performance for the SVM-based MPM with respect to the NB-based MPM, as shown in Table 3.

4.4. Discussion

In many countries, the mining sector has been an essential contributor towards their economic gains. Thus, the delineation of prospectively new regions of mineral occurrence is very important in

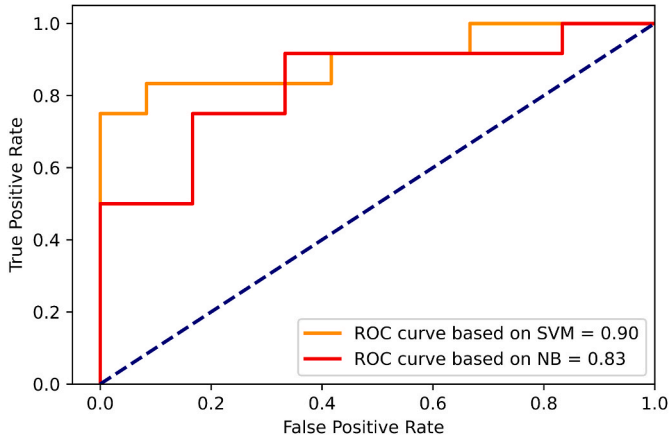

Fig. 8. Receiver operating characteristics (ROC) curve for the predictive models.

Table 3
Predictive performance of machine learning-based mineral prospectivity models.

Evaluation Metrics	SVM-based MPM	NB-based MPM
Precision	83.33%	81.25%
Recall	83.33%	72.20%
Accuracy	83.33%	76.50%
F1 Score	83.33%	77.80%

complementing efforts geared towards creating sustainable jobs for the unemployed, improving life expectancy, and providing essential infrastructure in the health and education sectors (Walser, 2002; Hosseinpour et al., 2022). The delineation of prospectively new areas of mineralisation occurrences (known as mineral prospectivity mapping) is achieved by collecting, analysing, and synthesising several layers sourced from geological, geophysical, and remote sensing datasets over a region of interest. Synthesising layers for MPM has been realised through the use of heuristic or knowledge driven (Abedi et al., 2012b; Du et al., 2016; Amponsah et al., 2022b; Forson and Menyeh, 2023), bivariate (Zhang et al., 2014; Harris et al., 2015), and multivariate (Xiong et al., 2018; Xu et al., 2021) methods.

In this study, machine learning (multivariate) methods comprising the SVM and the NB were adopted for the integration of thirteen geoscientifically-sourced thematic layers for the onward generation of predictive models that depict regions of potential mineral occurrences

over the Gomoa Area of Ghana's Southern Kibi-Winneba belt based on a number of reasons: (a) machine learning methods are statistically objective, reproducible, and are able to analyse the influence of the thematic layers towards mineralisation occurrence in a quantitative manner; (b) machine learning-based predictive modeling is less time consuming and relatively easy to carry out in comparison with the conventional methods (heuristic and bivariate methods) (Youssef and Pourghasemi, 2021); (c) the accuracy of machine learning-based predictive models generated are better than the conventional methods; and (d) the use of machine learning models in mineral prospectivity mapping within Ghana and West Africa is rare in literature. It is noteworthy that, the SVM and NB are not without defects when employed in predictive modeling. In the case of the SVM classifier, its execution capability is flawed in situations where the target classes overlap. SVM would also underperform in a situation where a large amount of data is involved. It also performs poorly when there is an imbalance between the training datasets (Deng et al., 2017). The reliability of the Naive Bayes classifier is greatly affected in a situation where the distribution of the thematic layers and the training datasets differ significantly, and thus its functionality requires the attributes (layers) to be independent (Tien Bui et al., 2012). This makes the NB classifier susceptible to the embedment of elicit subtle patterns in geoscientific datasets (Naghibi et al., 2017). In view of this, this study was further set out to compare the results of MPMs produced based on the SVM and NB as well as their predictive performance. Results obtained for the model evaluation metrics comprising AUC score, precision, recall, accuracy, and F1 score (Table 3 and Fig. 8) indicate that, although both the SVM and the NB models showed good performance, the SVM-based MPM was observed to exhibit an improved performance over the NB-based MPM. This further suggests that the delineated prospective zones (Fig. 5(a) and (b)) generally contained a high proportion of the number of known Au occurrences within the target labels, whereas the non-prospective zones were characterized by a greater proportion of non-Au occurrences.

5. Conclusion

As a preliminary step in mineral exploration programmes, it is desirable to efficiently evaluate the mineral prospect over an area of interest for its sufficient availability and optimum utilisation by adopting efficient machine learning approaches. Thus, in this study, two machine learning classifiers comprising support vector machines and naive bayes have been employed on thirteen input layers derived from geophysical, remote sensing, and geological datasets over the Gomoa Area of the Kibi-Winneba belt of Ghana to generate models that classify the various mineral prospective zones within the study area. The results obtained for the mineral prospectivity model produced based on the naive nayes classifier indicate that 35.97% of the total study area size (representing an areal extent of 296.02 km^2) was delineated as prospective, whereas in the case of the SVM-based mineral prospectivity model, 22.07% of the study area (with an area size of 181.62 km^2) was deemed prospective. Assessing the performance of a predictive model created is essential, as it emphasises confidence in the output produced. Hence, the area under the receiver operating characteristics curve, which is a standard statistical evaluation technique, was employed on the two MPMs generated. AUC scores obtained for the predictive models in this study indicate that the SVM-based MPM and NB-based MPM produced showed good prediction ability, with AUC scores of 0.90 and 0.83, respectively. However, the SVM-based MPM is the best at accurate prediction of mineral prospectivity zones within the study area. Thus, the use of the support vector machine and the naive bayes classifiers can be applied in other geological terranes for the accurate prediction of mineral prospective zones.

Declaration of competing interest

The authors declare that they have no known competing financial interests or personal relationships that could have appeared to influence the work reported in this paper.

Data availability

Data will be made available on request.

Acknowledgements

Authors are grateful to the University of Ghana-Carnegie Corporation and Building a New Generation Africa (BaNGA-Africa) for their immense support in making this study a success. Authors also wish to thank the United States Geological Survey Earth Resources Observation and Science Centre, Geodita Resources Limited, and GFZ German Research Centre for Geoscience (Potsdam-Germany) for making data available for use in this study. Authors are also thankful for the three anonymous reviewers for reviewing our paper. Their comments were vital to improving the manuscript.

References

Abedi, M., Norouzi, G.-H., Bahroudi, A., 2012a. Support vector machine for multi-classification of mineral prospectivity areas. Comput. Geosci. 46, 272–283.
Abedi, M., Torabi, S.A., Norouzi, G.-H., Hamzeh, M., Elyasi, G.-R., 2012b. Promethee ii: a knowledge-driven method for copper exploration. Comput. Geosci. 46, 255–263.
Agyei Duodu, J., Loh, G., Boamah, K., Baba, M., Hirdes, W., Toloczyki, M., Davis, D., 2009. Geological Map of Ghana 1: 1 000 000. Geological Survey Department.
Al-Kindi, K.M., Janizadeh, S., 2022. Machine learning and hyperparameters algorithms for identifying groundwater aflaj potential mapping in semi-arid ecosystems using lidar, sentinel 2, GIS data, and analysis. Rem. Sens. 14 (21), 5425.
Ama Salah, I., Liégeois, J.-P., Pouclet, A., 1996. Evolution d'un arc insulaire océanique birimien précoce au liptako nogérien (sirba): géologie, géochronologie et géochimie. J. Afr. Earth Sci. 22, 235–254.
Amponsah, P.O., Kwayisi, D., Awunyo, E.K., Sapah, M.S., Sakyi, P.A., Su, B.X., Lu, Y., Nude, P.M., 2023. New evidence for crustal reworking and juvenile arc-magmatism during the Palaeoproterozoic Eburnean events in the Suhum Basin, South-east Ghana. Geol. J. In Press.
Amponsah, P.O., Salvi, S., Béziat, D., Siebenaller, L., Baratoux, L., Jessell, M.W., 2015. Geology and geochemistry of the shear-hosted julie gold deposit, nw Ghana. J. Afr. Earth Sci. 112, 505–523.
Amponsah, P.O., Salvi, S., Didier, B., Baratoux, L., Siebenaller, L., Jessell, M., Nude, P.M., Gyawu, E.A., 2016. Multistage gold mineralization in the wa-lawra greenstone belt, nw Ghana: the bepkong deposit. J. Afr. Earth Sci. 120, 220–237.
Amponsah, P.O., Forson, E.D., 2023. Geospatial modeling of mineral potential zones using data-driven based weighting factor and statistical index techniques. J. Afr. Earth Sci., 105020
Amponsah, P.O., Forson, E.D., Sungzie, P.S., Loh, Y.S.A., 2022a. Groundwater Prospectivity Modeling over the Akatsi Districts in the Volta Region of ghana Using the Frequency Ratio Technique. Modeling Earth Systems and Environment, pp. 1–19.
Amponsah, T.Y., Danuor, S.K., Wemegah, D.D., Forson, E.D., 2022b. Groundwater potential characterisation over the voltaian basin using geophysical, geological, hydrological and topographical datasets. J. Afr. Earth Sci. 192, 104558.
Anum, S., Sakyi, P.A., Su, B.-X., Nude, P.M., Nyame, F., Asiedu, D., Kwayisi, D., 2015. Geochemistry and geochronology of granitoids in the kibi-asamankese area of the kibi-winneba volcanic belt, southern Ghana. J. Afr. Earth Sci. 102, 166–179.
Asiedu, D.K., Agoe, M., Amponsah, P.O., Nude, P.M., Anani, C.Y., 2019. Geochemical constraints on provenance and source area weathering of metasedimentary rocks from the paleoproterozoic (~ 2.1 ga) wa-lawra belt, southeastern margin of the west african craton. Geodin. Acta 31 (1), 27–39.
Bachri, I., Hakdaoui, M., Raji, M., Teodoro, A.C., Benbouziane, A., 2019. Machine learning algorithms for automatic lithological mapping using remote sensing data: a case study from souk arbaa sahel, sidi ifni inlier, western anti-atlas, Morocco. ISPRS Int. J. Geo-Inf. 8 (6), 248.
Baratoux, L., Metelka, V., Naba, S., Jessell, M.W., Grégoire, M., Ganne, J., 2011. Juvenile Paleoproterozoic crust evolution during the eburnean orogeny (2.2–2.0 ga), western Burkina Faso. Precambrian Res. 191 (1–2), 18–45.
Bédard, É., de Vazelhes, V.D.B., Beaudoin, G., 2022. Performance of predictive supervised classification models of trace elements in magnetite for mineral exploration. J. Geochem. Explor. 236, 106959.
Bérubé, C.L., Olivo, G.R., Chouteau, M., Perrouty, S., Shamsipour, P., Enkin, R.J., Morris, W.A., Feltrin, L., Thiémonge, R., 2018. Predicting rock type and detecting hydrothermal alteration using machine learning and petrophysical properties of the canadian malartic ore and host rocks, pontiac subprovince, québec, Canada. Ore Geol. Rev. 96, 130–145.
Béziat, D., Bourges, F., Debat, P., Lompo, M., Martin, F., Tollon, F., 2000. A paleoproterozoic ultramafic-mafic assemblage and associated volcanic rocks of the boromo greenstone belt: fractionates originating from island-arc volcanic activity in the west african craton. Precambrian Res. 101 (1), 25–47.
Bonhomme, M., 1962. Contribution à l'étude géochronologique de la plate-forme de l'Ouest Africain. Imprimerie Louis-Jean.

Cao, J., Zhang, Z., Du, J., Zhang, L., Song, Y., Sun, G., 2020. Multi-geohazards susceptibility mapping based on machine learning?a case study in jiuzhaigou, China. Nat. Hazards 102, 851–871.
Cardoso-Fernandes, J., Teodoro, A., Lima, A., Roda-Robles, E., 2019. Evaluating the performance of support vector machines (svms) and random forest (rf) in li-pegmatite mapping: preliminary results. In: Earth Resources and Environmental Remote Sensing/GIS Applications X, vol. 11156. SPIE, pp. 146–157.
Cardoso-Fernandes, J., Teodoro, A.C., Lima, A., Roda-Robles, E., 2020. Semi-automatization of support vector machines to map lithium (li) bearing pegmatites. Rem. Sens. 12 (14), 2319.
Carranza, E.J.M., 2008. Geochemical Anomaly and Mineral Prospectivity Mapping in GIS. Elsevier.
Carranza, E.J.M., Laborte, A.G., 2016. Data-driven predictive modeling of mineral prospectivity using random forests: a case study in catanduanes island (Philippines). Nat. Resour. Res. 25 (1), 35–50.
Carranza, E., Hale, M., Faassen, C., 2008. Selection of coherent deposit-type locations and their application in data-driven mineral prospectivity mapping. Ore Geol. Rev. 33 (3–4), 536–558.
Chen, Y., Wu, W., 2017. Application of one-class support vector machine to quickly identify multivariate anomalies from geochemical exploration data. Geochem. Explor. Environ. Anal. 17 (3), 231–238.
Cheng, Y., Fu, L.-Y., 2022. Nonlinear seismic inversion by physics-informed caianiello convolutional neural networks for overpressure prediction of source rocks in the o shore xihu depression, east China. J. Petrol. Sci. Eng. 215, 110654.
Davis, D., Hirdes, W., Schaltegger, U., Nunoo, E., 1994. U-pb age constraints on deposition and provenance of birimian and gold-bearing tarkwaian sediments in Ghana, west africa. Precambrian Res. 67 (1–2), 89–107.
De Boissieu, F., Sevin, B., Cudahy, T., Mangeas, M., Chevrel, S., Ong, C., Rodger, A., Maurizot, P., Laukamp, C., Lau, I., et al., 2018. Regolith-geology mapping with support vector machine: a case study over weathered Ni-bearing peridotites, New Caledonia. Int. J. Appl. Earth Obs. Geoinf. 64, 377–385.
Deng, C., Pan, H., Fang, S., Konaté, A.A., Qin, R., 2017. Support vector machine as an alternative method for lithology classification of crystalline rocks. J. Geophys. Eng. 14 (2), 341–349.
Diatta, F., Ndiaye, P.M., Diène, M., Amponsah, P.O., Ganne, J., 2017. The structural evolution of the Dialé-Daléma basin, Kédougou-Kéniéba Inlier, eastern Senegal. J. Afr. Earth Sci. 129, 923–933.
Dove, K., 1991. Geology of the I = 4_field Sheets Nos. 29 and 31, Winneba SW and NW. Ghana Geological Survey Department, Accra. Archive Report 25.
Du, X., Zhou, K., Cui, Y., Wang, J., Zhang, N., Sun, W., 2016. Application of fuzzy analytical hierarchy process (ahp) and prediction-area (pa) plot for mineral prospectivity mapping: a case study from the dananhu metallogenic belt, xinjiang, nw China. Arabian J. Geosci. 9, 1–15.
Dzigbodi-Adjimah, K., 2004. The mineralogy and petrography of the ferruginous manganese rocks at mankwadzi, Ghana. J. Afr. Earth Sci. 38 (3), 293–315.
Feng, X., Wang, E., Ganne, J., Amponsah, P., Martin, R., 2018. Role of volcano-sedimentary basins in the formation of greenstone-granitoid belts in the west african craton: a numerical model. Minerals 8 (2), 73.
Feng, X., Wang, E., Amponsah, P.O., Ganne, J., Martin, R., Jessell, M.W., 2019. Effect of pre-existing faults on the distribution of lower crust exhumation under extension: numerical modelling and implications for NW Ghana. Geosci. J. 23, 961–975.
Feybesse, J.-L., Billa, M., Guerrot, C., Duguey, E., Lescuyer, J.-L., Milesi, J.-P., Bouchot, V., 2006. The paleoproterozoic ghanaian province: geodynamic model and ore controls, including regional stress modeling. Precambrian Res. 149 (3–4), 149–196.
Forson, E.D., Menyeh, A., 2023. Best worst method-based mineral prospectivity modeling over the central part of the southern kibi-winneba belt of Ghana. Earth Science Informatics 1–20.
Forson, E.D., Menyeh, A., Wemegah, D.D., Danuor, S.K., Adjovu, I., Appiah, I., 2020. Mesothermal gold prospectivity mapping of the southern kibi-winneba belt of Ghana based on fuzzy analytical hierarchy process, concentration-area (c-a) fractal model and prediction-area (p-a) plot. J. Geophys. 174, 103971.
Forson, E.D., Menyeh, A., Wemegah, D.D., 2021. Mapping lithological units, structural lineaments and alteration zones in the southern kibi-winneba belt of Ghana using integrated geophysical and remote sensing datasets. Ore Geol. Rev. 137, 104271.
Forson, E.D., Amponsah, P.O., Hagan, G.B., Sapah, M.S., 2022a. Frequency Ratio-Based Flood Vulnerability Modeling over the Greater Accra Region of ghana. Modeling Earth Systems and Environment, pp. 1–20.
Forson, E.D., Wemegah, D.D., Hagan, G.B., Appiah, D., Addo-Wuver, F., Adjovu, I., Otchere, F.O., Mateso, S., Menyeh, A., Amponsah, T., 2022b. Data-driven multi-index overlay gold prospectivity mapping using geophysical and remote sensing datasets. J. Afr. Earth Sci. 190, 104504.
Geodita Resources Ltd, 2007. Exploration Summary on the Gomoa Mangoase Licence (Unpublished internal report).
Geodita Resources Ltd, 2012. Trench Report on Gomoa Mangoase Concession (Unpublished internal report).
Geodita Resources Ltd, 2013. Drill Report on Gomoa Mangoase Concession (Unpublished internal report).
Ghana Limited, Newmont, 2006. Terminal Report on Gomoa Prospecting License (Pl3/66 (Unpublished internal report).
Harris, J., Grunsky, E., Behnia, P., Corrigan, D., 2015. Data-and knowledge-driven mineral prospectivity maps for Canada's north. Ore Geol. Rev. 71, 788–803.
Hirdes, W., Davis, D., Eisenlohr, B., 1992. Reassessment of proterozoic granitoid ages in Ghana on the basis of u/pb zircon and monazite dating. Precambrian Res. 56 (1–2), 89–96.
Hosseinpour, M., Osanloo, M., Azimi, Y., 2022. Evaluation of positive and negative impacts of mining on sustainable development by a semi-quantitative method. J. Clean. Prod. 366, 132955.
Jessell, M.W., Amponsah, P.O., Baratoux, L., Asiedu, D.K., Loh, G.K., Ganne, J., 2012. Crustal-scale transcurrent shearing in the paleoproterozoic Sefwi-Sunyani-Comoe region, West Africa. Precambrian Res. 212, 155–168.
Klemd, R., Hünken, U., Olesch, M., 2002. Metamorphism of the country rocks hosting gold–sulfide-bearing quartz veins in the paleoproterozoic southern kibi-winneba belt (se-Ghana). J. Afr. Earth Sci. 35 (2), 199–211.
Ledru, P., Milési, J., Vinchon, C., Ankrah, P., Johan, V., Marcoux, E., 1988. Geology of the birimian series of Ghana. In: International Conference and Workshop on the Geology of Ghana with Special Emphasis on Gold Programme and Abstracts. Accra, Ghana, pp. 26–27.
Leube, A., Hirdes, W., Mauer, R., Kesse, G.O., 1990. The early proterozoic birimian supergroup of Ghana and some aspects of its associated gold mineralization. Precambrian Res. 46 (1–2), 139–165.
Li, X., Sun, Y., 2020. Stock intelligent investment strategy based on support vector machine parameter optimization algorithm. Neural Comput. Appl. 32, 1765–1775.
Liu, Z., Xu, J., Liu, M., Yin, Z., Liu, X., Yin, L., Zheng, W., 2023. Remote Sensing and Geostatistics in Urban Water-Resource Monitoring: A Review. Marine and Freshwater Research.
Lüdtke, G., Hirdes, W., Konan, K., Koné, Y., N'Da, D., Traoré, Y., Zamblé, Z., de la Géologie, D., et al., 2000. Géologie de la region haute comoe sud/geology of the haute-comoe south area.
Ma, J., Xia, D., Wang, Y., Niu, X., Jiang, S., Liu, Z., Guo, H., 2022. A comprehensive comparison among metaheuristics (mhs) for geohazard modeling using machine learning: insights from a case study of landslide displacement prediction. Eng. Appl. Artif. Intell. 114, 105150.
McKay, G., Harris, J., 2016. Comparison of the data-driven random forests model and a knowledge-driven method for mineral prospectivity mapping: a case study for gold deposits around the huritz group and nueltin suite, nunavut, Canada. Nat. Resour. Res. 25 (2), 125–143.
Milési, J.-P., Ledru, P., Feybesse, J.-L., Dommanget, A., Marcoux, E., 1992. Early proterozoic ore deposits and tectonics of the birimian orogenic belt, west Africa. Precambrian Res. 58 (1–4), 305–344.
Naghibi, S.A., Moghaddam, D.D., Kalantar, B., Pradhan, B., Kisi, O., 2017. A comparative assessment of GIS-based data mining models and a novel ensemble model in groundwater well potential mapping. J. Hydrol. 548, 471–483.
Noble, W.S., 2006. What is a support vector machine? Nat. Biotechnol. 24 (12), 1565–1567.
Nunoo, S., Hofmann, A., Kramers, J., 2022. Geology, zircon U–Pb dating and εHf data for the Julie greenstone belt and associated rocks in NW Ghana: implications for Birimian-to-Tarkwaian correlation and crustal evolution. J. Afr. Earth Sci. 186, 104444.
Opare-Addo, E., Browning, P., John, B., 1993. Pressure-temperature constraints on the evolution of an early Proterozoic plutonic suite in southern Ghana, west africa. J. Afr. Earth Sci. 17 (1), 13–22.
Parsa, M., Maghsoudi, A., 2021. Assessing the e ects of mineral systems-derived exploration targeting criteria for random forests-based predictive mapping of mineral prospectivity in Ahar-Arasbaran area, Iran. Ore Geol. Rev. 138, 104399.
Pedregosa, F., Varoquaux, G., Gramfort, A., Michel, V., Thirion, B., Grisel, O., Blondel, M., Prettenhofer, P., Weiss, R., Dubourg, V., Vanderplas, J., Passos, A., Cournapeau, D., Brucher, M., Perrot, M., Duchesnay, E., 2011. Scikit-learn: machine learning in Python. J. Mach. Learn. Res. 12, 2825–2830.
Perrouty, S., Aillères, L., Jessell, M.W., Baratoux, L., Bourassa, Y., Crawford, B., 2012. Revised Eburnean geodynamic evolution of the gold-rich southern ashanti belt, Ghana, with new field and geophysical evidence of pre-Tarkwaian deformations. Precambrian Res. 204, 12–39.
Pham, B.T., Jaafari, A., Van Phong, T., Mafi-Gholami, D., Amiri, M., Van Tao, N., Duong, V.-H., Prakash, I., 2021. Naïve bayes ensemble models for groundwater potential mapping. Ecol. Inf. 64, 101389.
Porwal, A., Carranza, E.J.M., Hale, M., 2006. Bayesian network classifiers for mineral potential mapping. Comput. Geosci. 32 (1), 1–16.
Rodriguez-Galiano, V., Sanchez-Castillo, M., Chica-Olmo, M., Chica-Rivas, M., 2015. Machine learning predictive models for mineral prospectivity: an evaluation of neural networks, random forest, regression trees and support vector machines. Ore Geol. Rev. 71, 804–818.
Saberioon, M., Císar, P., Labbé, L., Soucek, P., Pelissier, P., Kerneis, T., 2018. Comparative performance analysis of support vector machine, random forest, logistic regression and k-nearest neighbours in rainbow trout (oncorhynchus mykiss) classification using image-based features. Sensors 18 (4), 1027.
Salvi, S., Amponsah, P.O., Siebenaller, L., Béziat, D., Baratoux, L., Jessell, M., 2016. Shear-related gold mineralization in Northwest Ghana: the Julie deposit. Ore Geol. Rev. 78, 712–717.
Sapah, M.S., Agbetsoamedo, J.E., Amponsah, P.O., Dampare, S.B., Asiedu, D.K., 2021. Neodymium isotope composition of palaeoproterozoic birimian shales from the wa-lawra belt, north-west Ghana: constraints on provenance. Geol. J. 56 (4), 2072–2081.
Shabankareh, M., Hezarkhani, A., 2017. Application of support vector machines for copper potential mapping in kerman region, Iran. J. Afr. Earth Sci. 128, 116–126.
Shirmard, H., Farahbakhsh, E., Müller, R.D., Chandra, R., 2022. A review of machine learning in processing remote sensing data for mineral exploration. Rem. Sens. Environ. 268, 112750.
Sun, T., Chen, F., Zhong, L., Liu, W., Wang, Y., 2019. Gis-based mineral prospectivity mapping using machine learning methods: a case study from tongling ore district, eastern China. Ore Geol. Rev. 109, 26–49.

Sun, T., Li, H., Wu, K., Chen, F., Zhu, Z., Hu, Z., 2020. Data-driven predictive modelling of mineral prospectivity using machine learning and deep learning methods: a case study from southern Jiangxi Province, China. Minerals 10 (2), 102.
Tien Bui, D., Pradhan, B., Lofman, O., Revhaug, I., 2012. Landslide susceptibility assessment in vietnam using support vector machines, decision tree, and naive bayes models. Math. Probl. Eng. 20 (12), 2012.
Vapnik, V., 1999. The Nature of Statistical Learning Theory. Springer Science & Business Media.
Wemegah, D.D., Preko, K., Noye, R.M., Boadi, B., Menyeh, A., Danuor, S.K., Amenyoh, T., et al., 2015. Geophysical interpretation of possible gold mineralization zones in kyerano, south-western Ghana using aeromagnetic and radiometric datasets. J. Geosci. Environ. Protect. 3 (4), 67.
Xiong, Y., Zuo, R., Carranza, E.J.M., 2018. Mapping mineral prospectivity through big data analytics and a deep learning algorithm. Ore Geol. Rev. 102, 811–817.
Xtra-Gold Resource Corporation, 2021. Kibi Gold Project. Exploration report.
Xu, Y., Li, Z., Xie, Z., Cai, H., Niu, P., Liu, H., 2021. Mineral prospectivity mapping by deep learning method in yawan-daqiao area, gansu. Ore Geol. Rev. 138, 104316.
Youssef, A.M., Pourghasemi, H.R., 2021. Landslide susceptibility mapping using machine learning algorithms and comparison of their performance at abha basin, asir region, Saudi Arabia. Geosci. Front. 12 (2), 639–655.
Zeghouane, H., Allek, K., Kesraoui, M., 2016. Gis-based weights of evidence modeling applied to mineral prospectivity mapping of sn-w and rare metals in laouni area, central hoggar, Algeria. Arabian J. Geosci. 9 (5), 1–13.
Zhan, C., Dai, Z., Yang, Z., Zhang, X., Ma, Z., Thanh, H.V., Soltanian, R.M., 2023. Subsurface sedimentary structure identification using deep learning: a review. Earth Sci. Rev. 239, 104370.
Zhang, Y., Liu, L., 2019. Temporal point pattern analysis of human activities using gis methods: a case study of library visiting activities in chengdu city, China. Prof. Geogr. 71 (4), 738–750.
Zhang, D., Agterberg, F., Cheng, Q., Zuo, R., 2014. A comparison of modified fuzzy weights of evidence, fuzzy weights of evidence, and logistic regression for mapping mineral prospectivity. Math. Geosci. 46, 869–885.
Zhang, L., Huang, M., Li, M., Lu, S., Yuan, X., Li, J., 2021. Experimental study on evolution of fracture network and permeability characteristics of bituminous coal under repeated mining e ect. Natural Resources Research, pp. 1–24.
Zuo, R., Carranza, E.J.M., 2011. Support vector machine: a tool for mapping mineral prospectivity. Comput. Geosci. 37 (12), 1967–1975.
Zuo, R., Carranza, E.J.M., Wang, J., 2016. Spatial analysis and visualization of exploration geochemical data. Earth Sci. Rev. 158, 9–1.